Proceedings of CONF-MSS 2026 Symposium: Advanced Composite Materials and Polymer Chemistry
DOI: 10.54254/2755-2721/2026.AD33154

Comparative Analysis of the Influence of Airfoil Thickness on Aerodynamic Performance at High Reynolds Numbers

Qinghan Yan

School of Mechanics and Civil Engineering, Jinan University, Guangzhou, China
yqh103140@stu2023.jnu.edu.cn

Abstract. The paper is a numerical simulation analysis of a NACA2410 and NACA2412 airfoil under a Reynolds number of 2.2×10^6 in two dimensions. The airfoil geometric model occurred based on the computational fluid dynamics (CFD) numerical simulation technology of the finite volume method, and the grid of the computational domain was divided, and the corresponding calculations of the simulation solution were performed. Six groups of attack angles of -8 °, -4°, 0°, 4°, 8° and 12° were selected for simulation. The results point out that the lift coefficient of NACA2412 airfoil is slightly greater than the lift coefficient of NACA2410 airfoil in all angles of attack, and the difference in lift coefficient of the two airfoils increases as the angle of attack (AOA) increases. At the AOA of -8 to 8 degrees and NACA2412 has a brighter drag coefficient at large AOA of 12 degrees, the drag coefficient of NACA2410 is less than the NACA2412. Comparison of lift and drag characteristics of two airfoils has demonstrated that the thickness of the airfoil affects aerodynamic performance in high Reynolds number which forms a basis of subsequent reference in the future of airfoil design and airfoil selection.

Keywords: NACA airfoil, Computational fluid dynamics (CFD) numerical simulation, Aerodynamic characteristics

1. Introduction

Drones have been widely used in logistics transportation, national defense security and disaster relief and rescue, owing to their advantages, which are flexibility, efficiency and low cost, in the last ten years. As early as the 1930s, the National Advisory Committee for Aeronautics (NACA) developed airfoils suitable for flight under different conditions, which are widely applied in the current aviation industry. Among numerous airfoils, NACA 2410 and NACA 2412 are widely used in UAV design because of their unique aerodynamic characteristics. For four-digit coded airfoils, camber and thickness are important parameters affecting the aerodynamic characteristics of the airfoil [1,2].

The differences in the performance of the two airfoils can be identified through numerical studies of the two airfoil NACA 2410 and NACA 2412. The aerodynamic performance of these two airfoils has been the subject of study of many scholars at the moment. The aerodynamic properties of NACA 2410 morphing camber wing variant were investigated by SARJITO and AKLIS N [3]. Ravichandrakumar, KB et al. investigated the aerodynamic nature of the rotating leading edge of

© 2026 The Authors. This is an open access article distributed under the terms of the Creative Commons Attribution License 4.0 (https://creativecommons.org/licenses/by/4.0/).

DOI: 10.54254/2755-2721/2026.AD33154

NACA 2412 [4]. Though the use of the two airfoils is already highly widespread, few systematic comparative studies aiming at them exist, and hence it is not possible to intuitively expose the differences in their aerodynamic properties at high Reynolds numbers.

The paper aims at conducting the systematic comparative study of aerodynamic characteristics of the NACA 2410 and NACA 2412 airfoils at high Reynolds numbers. This study employs computational modeling to determine the influence of the span of thickness of an airfoil on its aero-performance. In particular, it examines the variations in drag and lift factors, as well as such properties of the flow field as the speed and pressure profiles over an incident angle range. It naturally shows the increased lift properties of a high angle of attack and the structural integrity with added thickness. The research work of this paper does not only complement the relevant simulation data of NACA airfoils, but also provides a scientific guiding base and engineering point of reference over the best design and choice of the UAV airfoils, in regards to the high Reynolds numbers.

2. Numerical simulation

2.1. Geometric model and computational domain

To achieve the calculation for NACA 2410 and NACA 2412, Figure 1 presents the geometric models of the two airfoils; meanwhile, to ensure calculation accuracy and simulation precision, the models can be constructed after dividing their curves into figures composed of multiple points [5].

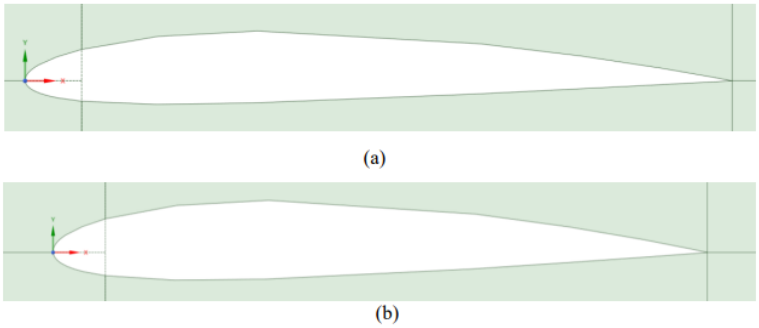

Figure 1. : Airfoil geometric model, (a) NACA 2410; (b) NACA 2412（picture credit : original）

2.2. Mesh generation

The C-type computational domain model of the airfoil is illustrated in Figure 2 and the inlet part is defined as the inlet velocity and the outlet part is defined as the outlet pressure. This model consists of a square whose side dimensions measure 1.5m and a semicircle whose diameter measures 1.5m that are cut together which is capable of capturing the leading and trailing edges of the airfoil, thus resulting in relatively accurate simulation results [6]. The C-type computational domain may be subdivided into six regions to generate a mesh of the airfoil more conveniently. There are four regions in particular that are separated by the leading and trailing edges based on orthogonal positions, and the upper-left and lower-left arc segments based on the vertical segmentation method [7]. Lastly, the region boundaries and faces obtained are made size-adjustments and the corresponding parameters are presented in Table 1.

DOI: 10.54254/2755-2721/2026.AD33154

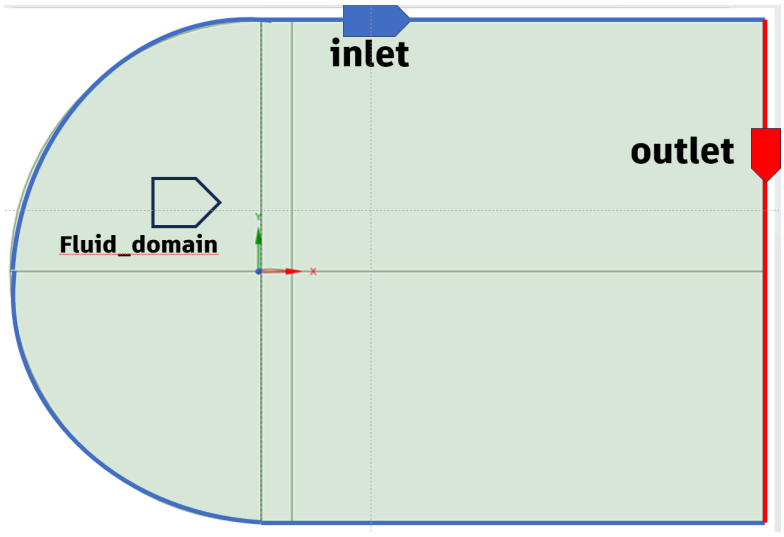

Figure 2. Airfoil computational domain model (picture credit: original)

Table 1. Grid division parameters

Number of partitions (/ sides)	300
Type of deviation	First concentrated, then dispersed
Deviation factor	40000

Regarding the mesh generation of the airfoil computational domain, the mesh adopts a multi-zone refinement strategy. The external computational domain uses a 0.4 m uniform mesh; the airfoil wall and near-field regions adopt a refined mesh of 3×10^{-4} m. The overall mesh generation result is shown in Figure 3, and the local refinement details of the airfoil are shown in Figure 4.

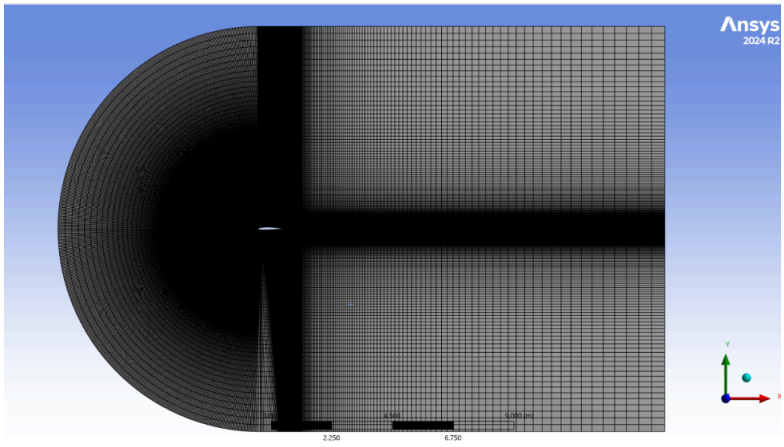

Figure 3. Computational domain grid division (picture credit: original)

DOI: 10.54254/2755-2721/2026.AD33154

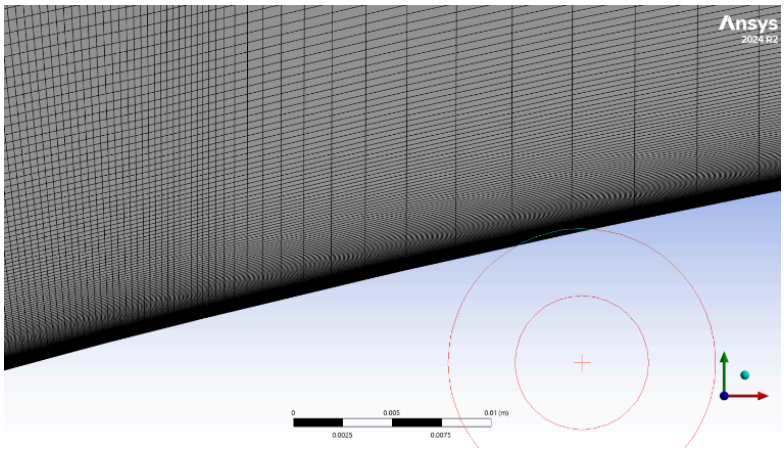

Figure 4. Local details around the wing shape（picture credit : original）

Boundary Conditions and governing equations. The number of iterations needed to get relatively accurate results to this simulation is 1000 and the residual is 10^{-6}. The fundamental governing equations used in the given paper include the incompressible continuity equation and the Navier-Stokes equations. The continuity equation can be expressed as follows.

$$\frac{\partial \rho}{\partial t} + \frac{\partial \rho u}{\partial x} + \frac{\partial \rho v}{\partial y} + \frac{\partial \rho w}{\partial z} = 0 \tag{1}$$

Where the variable ρ accounts for fluid density, u、 v and w define velocity gradients across the x、y and z coordinate system.

The Navier-Stokes equation can be represented as in Equation (2).

$$\rho \frac{\partial \mathbf{V}}{\partial t} + \rho\left((\mathbf{V}\cdot)\mathbf{V}\right)\mathbf{V} = -\nabla \rho + \rho g + \nabla \cdot \tau \tag{2}$$

Where V is the velocity vector; τ is the internal friction force produced by the viscosity of the molecules of the fluid; g is the acceleration due to gravity.

This paper uses the lift and drag coefficient to determine the aerodynamic performance of the airfoil and the formula equations of the lift coefficient and the drag coefficient are as follows [8].

$$C_L = \frac{F_L}{1/2\rho V^2 A} \tag{3}$$

$$C_D = \frac{F_D}{1/2\rho V^2 A} \tag{4}$$

Where F_L is the lift force on the wing, $F_D$is the drag force on the wing, A is the wing area.

Furthermore, the flux to be used in the simulation is second-order upwind, the pressure-velocity coupling scheme chosen is Coupled, and the K- omega SST model is selected to be used in numerical calculation [9,10]. Table 2 contains the settings of the rest of the boundary conditions.

DOI: 10.54254/2755-2721/2026.AD33154

Table 2. Physical conditions of the boundary layer

Parameters	Values
Reynolds number	2.2×106
Gas density ρ (kg/m³)	1.225
Viscosity (kg/m·s)	1.7894e5
Turbulence ratio	0.1
Import speed (m/s)	33
Turbulent scale	0.3

3. Results and discussion

3.1. Comparative analysis of aerodynamic characteristics

Figures 5 and 6 respectively provide the change in the lift and drag coefficient with the angle of attack (AOA) of the two airfoils. As observed in the two figures, the lift coefficient curves of the two airfoils rise linearly with the AOA in the range of -8 ° to 12°. The lift characteristics of the two are very near within the test range.

In particular, in most attack angles the drag coefficient of NACA 2412 (thicker airfoil) is marginally greater than that of NACA 2410. The drag coefficient of NACA 2410 is a little greater at maximum AOA (12°) which could be associated with the drag separation properties of the airfoil at large angles of attack. The difference in the drag coefficient of the two airfoils is quite minimal and this means the addition of the 10 percent to 12 percent thickness does not have a significant impact on the drag.

Besides, to see the variations of aerodynamic features in a more detailed manner, Figure 7 and Figure 8 provide the relevant bar chart variations. Based on these two figures, it can be observed that as the AOA is increased the difference between the two lift characteristics of the two decreases gradually and the performance of NACA 2412 increases gradually compared to that of NACA 2410 with the difference becoming more and more apparent.

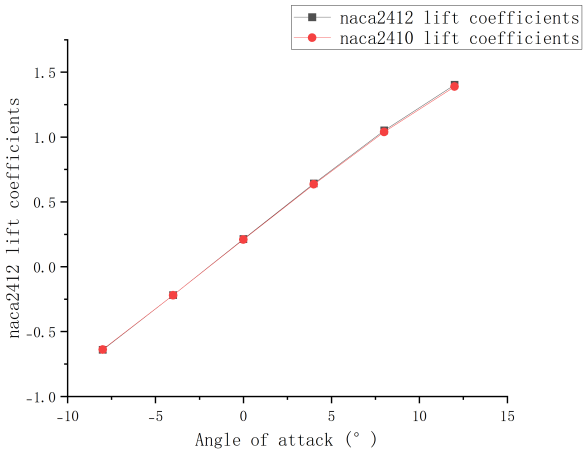

Figure 5. Comparison of lift coefficients between NACA 2410 and NACA 2412 (picture credit: original)

DOI: 10.54254/2755-2721/2026.AD33154

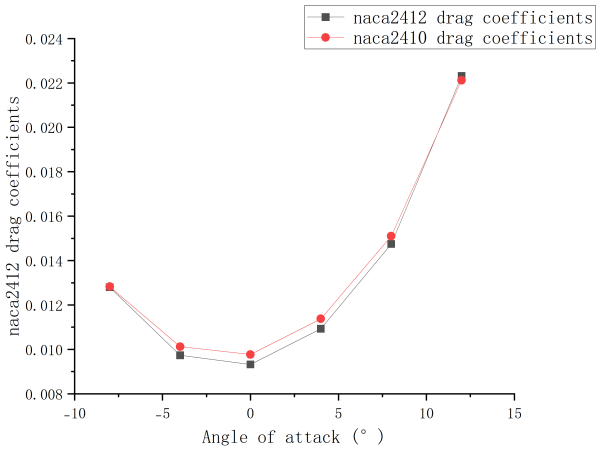

Figure 6. Comparison of drag coefficients between NACA 2410 and NACA 2412 (picture credit : original)

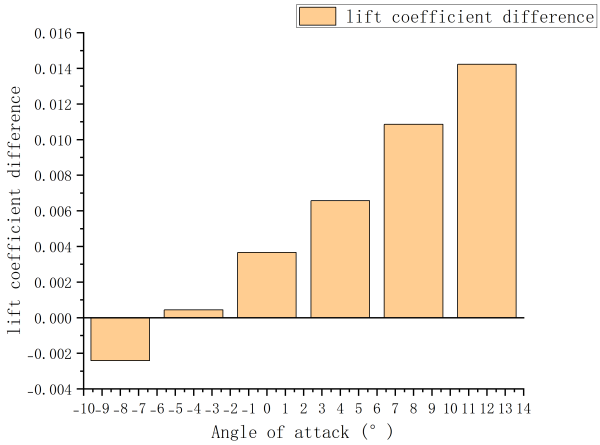

Figure 7. Comparison of lift coefficient difference bar charts between NACA 2410 and NACA 2412 (picture credit: original)

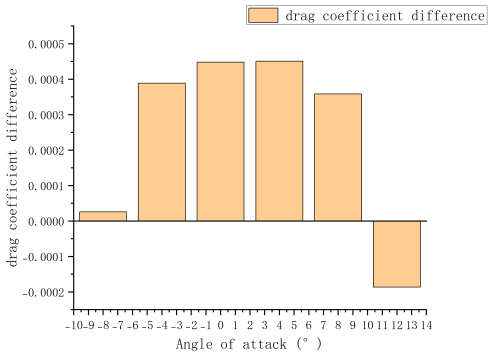

Figure 8. Comparison of lift coefficient difference bar charts between NACA 2410 and NACA 2412 (picture credit : original)

DOI: 10.54254/2755-2721/2026.AD33154

3.2. Comparative analysis of velocity distribution contours

Figure 9 shows the velocity distribution within the flow field of the two NACA 2410 and NACA 2412 airfoils at the above different angles of attack. According to Figure 9, the curves of velocity of the two airfoils show the principle rule that the larger the AOA, the larger the area of the high velocity on the airfoil upper surface and the greater the value of velocity. At positive angles of attack, a high-velocity low-pressure area is present on the upper surface of the airfoil and a low-velocity high-pressure area on the lower surface; at negative angles of attack the distribution of the velocity on the upper and lower surfaces of the airfoil is less sharp. But in the case of NACA 2412 airfoil at the large angles of 8 and 12 degrees of attack the longitudinal coverage of the zone of high velocity on the upper surface is considerably more than in the case of NACA 2410. The impact of this is that, as the AOA increases, the thick airfoil has the capacity to create the high velocity area without reducing the speed of the moving air hence the provision of flow fields to enhance lift.

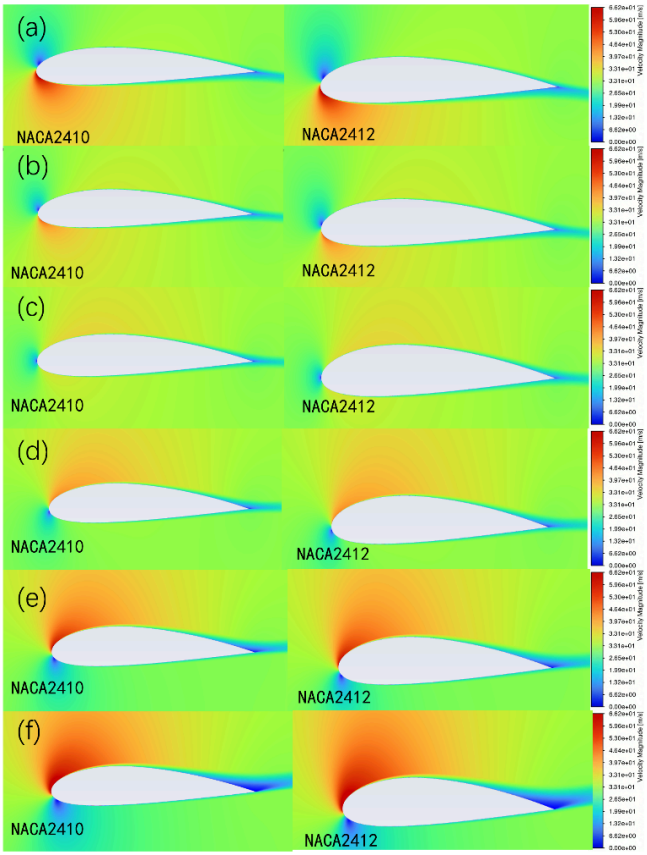

Figure 9. Velocity distribution contours of NACA 2410 and NACA 2412 at different AOAs, (a) -8°; (b) -4°; (c) 0°; (d) 4°; (e) 8°; (f) 12° (picture credit: original)

3.3. Comparative analysis of pressure contours

Figure 10 indicates that the lines of pressure in the two airfoils obey the law of increasing the difference between pressure on the upper and lower surfaces with the AOA. The difference in pressure between two faces, which one is the upper one, the other is the lower one of the two is quite small at negative angles of attack; very large at angles of attack that are above zero. The low-pressure region of the upper part of the NACA 2412 airfoil area is larger and the high-pressure

DOI: 10.54254/2755-2721/2026.AD33154

region area of the lower part is smaller and more concentrated and the pressure difference between the bottom and top sides is also higher than NACA 2410.

Moreover, it is also possible to notice uniformity of the flow field of the contours in order to identify the phenomena of the flow separation. Figure 10(f) indicates that the disordered regions and uneven distribution of pressure are located at the trailing end of the airfoil at NACA 2410, 12 °angle of attack, which implies that the separation of the flow in the airfoil takes place at the trailing end, and it results in the growth of the drag coefficient.

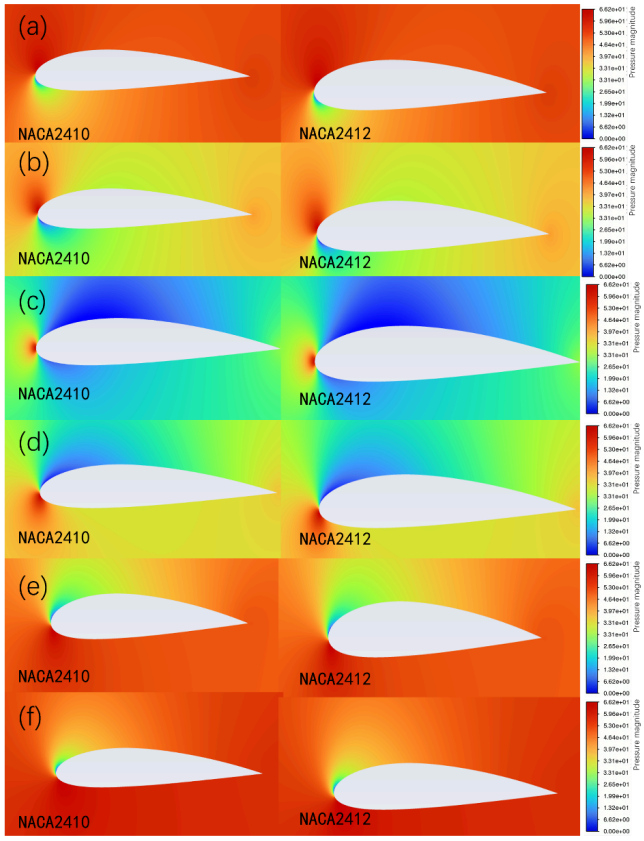

Figure 10. Pressure distribution contours of NACA 2410 and NACA 2412 at different AOAs, (a) -8°; (b) -4°; (c) 0°; (d) 4°; (e) 8°; (f) 12°（picture credit : original）

4. Conclusion

The paper applies the computational fluid dynamics (CFD) numerical method of simulation to perform a comparative analysis of aerodynamic characteristics of NACA 2410 and NACA 2412 airfoils at angles of attack ranging between -8 and 12 degrees under a high Reynolds number ($Re=2.2\times10^6$) to establish how airfoil thickness can influence the lift and drag and distributions of the flow field. The overall findings are as follows:

The test range shows that the lift coefficients of the two airfoils are linearly related to the AOA in the light of the coefficient which is concerned about lift and curves have similar trends. The coefficient which is about lift, of NACA 2412 is much bigger than the one of NACA 2410 at the angles of attack considered and the difference between the lift coefficient of the two planes. This means that lift advantage of the thicker airfoil is more prominent at large AOA.

From the point of view of comparing the drag coefficient ,it's clear that the trend of the drag coefficient versus the AOA of both the airfoils at the test range is the same and the curves are highly

DOI: 10.54254/2755-2721/2026.AD33154

overlapping in regards to the behaviour of the drag of the two airfoils, which implies the behaviour of the drag of the two NACA 2410 and the NACA 2412 at the test range is similar. When they are in demand, NACA 2412 can result in a slight increase in structural strength and slight or no structural performance degradation.

NACA 2412 may be a bit weaker in structure than in case the weight and structural requirements are both high, and much more applicable in case of a weight structural demand ratio, though of higher aerodynamic characteristics.

References

[1] Zhang, J., et al. (2025). Low-altitude unmanned aerial vehicle technology: Current status and prospects. Strategic Study of CAE, 27, 73-85.
[2] Sarjito, A., Aklis, N. and Hartanto, T. (2017) An optimization of flap and slat angle airfoil NACA 2410 using CFD. AIP Conference Proceedings, 1831, 020015.
[3] Ravichandrakumar, K.B., Subramanian, L.R.G. (2024) Aerodynamic study of a leading-edge rotating cylinder in a cambered aerofoil (NACA2412). Aircraft Engineering and Aerospace Technology, 96(10), 1311-1320.
[4] Liu, H., et al. (2024). Aerodynamic performance optimization of H-type vertical-axis wind turbine based on CFD and Taguchi method. Advances in New & Renewable Energy, 12(6),634-641.
[5] Lee, H., Save, A., Seshadri, P., & Rauleder, J. (2025) Large airfoil models. Computers & Fluids, 298, 106662.
[6] Liu, J., et al. (2024) Afbench: A large-scale benchmark for airfoil design. Advances in Neural Information Processing Systems, 37, 82757-82780.
[7] Amirsalari, B., & Rocha, J. (2023) Recent advances in airfoil self-noise passive reduction. Aerospace, 10(9),1-49.
[8] Rezaeiha, A., Montazeri, H., & Blocken, B. (2019) On the accuracy of turbulence models for CFD simulations of vertical axis wind turbines. Energy, 180, 838-857.
[9] Alom, N., Saha, U. K., & Dewan, A. (2021) In the quest of an appropriate turbulence model for analyzing the aerodynamics of a conventional Savonius (S-type) wind rotor. Journal of Renewable and Sustainable Energy, 13(2), 023302.
[10] Baghdadi, M., Xi, G., & Jing, Y. (2022) Investigation of the aerodynamic performance of a vertical axis wind turbine using various turbulence models and experimental validation. Energy Conversion and Management, 258, 115533.